Refractivity Data Fusion

Ted Rogers
SPAWAR Systems Center, Pacific
53560 Hull Street
San Diego, CA 92152
phone: (619) 553-1416 email: ted.rogers@navy.mil

Peter Gerstoft and Caglar Yardim
University of California, San Diego
9500 Gilman Dr, La Jolla, CA 92093-0238
email: gerstoft@ucsd.edu

Award Number: N00014WX20503, N00014-13-1-0360
http://www.mpl.ucsd.edu/people/pgerstoft/

LONG-TERM GOALS

Fuse refractivity inferred from electromagnetic (EM) propagation observations with background fields from numerical weather prediction (NWP) models.

OBJECTIVES

Develop data fusion method for atmospheric refractivity scheme based on objective analysis. Develop means to map observations of refractivity based on RF propagation measurements into the space utilized for the analysis. Exercise the data fusion scheme on a combination of synthetic and real data to assess performance. Acheive reasonable processing time (on the order of 1-minute) with a representative domain size using a high-end laptop computer.

APPROACH

An initial approach to estimation of atmospheric surface layer parameters by fusing radar clutter data with ensemble predictions from NWP is described in [1]. That work was completed in the beginning of the 2013 Fiscal Year. We now describe a fusing EM observations with NWP background for the region above the surface layer (that includes surface based ducts and elevated ducts).

In fusing EM observations with background from NWP, some considerations include:

1. The mapping from the space of EM signal enhancement (typically dBs) into the space of modified refractivity is non-linear, sometimes highly so.
2. NWP output is in the space of refractivity as a function of three spatial dimensions and virtually all EM inverse method implementations (e.g., refractivity-from-clutter) are in the space of parameters such as the trapping layer height and the “M-deficit” (the change in refractivity across a trapping layer).
3. EM propagation is highly sensitive to the vertical displacement of features and performing the objective analysis in the space of Cartesian coordinates results in smearing when features in the

Report Documentation Page

Form Approved
OMB No. 0704-0188

1. REPORT DATE	2. REPORT TYPE	3. DATES COVERED
30 SEP 2013		**00-00-2013 to 00-00-2013**

4. TITLE AND SUBTITLE	5a. CONTRACT NUMBER
Refractivity Data Fusion	5b. GRANT NUMBER
	5c. PROGRAM ELEMENT NUMBER
6. AUTHOR(S)	5d. PROJECT NUMBER
	5e. TASK NUMBER
	5f. WORK UNIT NUMBER
7. PERFORMING ORGANIZATION NAME(S) AND ADDRESS(ES) **SPAWAR Systems Center, Pacific,53560 Hull Street,San Diego,CA,92152**	8. PERFORMING ORGANIZATION REPORT NUMBER
9. SPONSORING/MONITORING AGENCY NAME(S) AND ADDRESS(ES)	10. SPONSOR/MONITOR'S ACRONYM(S)
	11. SPONSOR/MONITOR'S REPORT NUMBER(S)

12. DISTRIBUTION/AVAILABILITY STATEMENT
Approved for public release; distribution unlimited

13. SUPPLEMENTARY NOTES

14. ABSTRACT

15. SUBJECT TERMS

16. SECURITY CLASSIFICATION OF:			17. LIMITATION OF ABSTRACT	18. NUMBER OF PAGES	19a. NAME OF RESPONSIBLE PERSON
a. REPORT **unclassified**	b. ABSTRACT **unclassified**	c. THIS PAGE **unclassified**	**Same as Report (SAR)**	**8**	

background (i.e., model predictions) and observations are displaced from one another.

Due to the degree of non-linearity in the problem, it is doubtful that a best approach can be analytically arrived at. Rather, how to best implement the problem of performing an objective analysis for refractivity is amenable to a variety of alternative approaches.

We implement a hybrid 3-and-2 dimensional variational analysis scheme (3D/2D-VAR) [2 and 3]. We start with the Cartesian representation of refractivity generated by the COAMPS model, referred to here as "prognostic" representation. We utilize diagnositc routines to find heights and modified refractivity values for inflection points associated with trapping layers for each vertical refractivity profile in the prognostic refractivity volume. The diagnostic variables facilitate direct operations on the heights and gradients of trapping layers. It should be noted, though, that diagnostic variables only represent the features that are important in EM propagation. For example, if a surface based duct were present with the top of the duct at 200 meters, then only the lower 200 meters of the refractivity profile would be characterized by the diagnostic variables – so it would not be unusual for the diagnostic variables to not contain features above 200-or-so meters These result is that the 3-D prognostic representation is augmented with a 2-D diagnostic representation. The mapping from the space of the prognostic values to the space of the diagnostic values is unique; that is not necessarily so in the other direction. The process flow in as follows:

1. COAMPS M-value fields are used to populate the prognostic background representation.
2. Diagnositic algorithms populate the dignostic background representation from the prognostic representation.
3. Observations of EM propagation are mapped into space of the diagnostic variables. The diagnostic variables include the height of the top of the trapping layer, the M-excess (the difference between the value of modified refractivity at the top of the layer and at the surface) and so-on; these are the quantities typically utilized in inversions of refractivity from signal power measurements and inversion of refractivity from radar clutter.
4. An objective analysis is performed in the space of the diagnostic variables. This results – as is the normal result for objective analysis – resulted in an adjustment in the 2-D representation of refractivity over the domain of the diagnosic variables.
5. In a step referred to as "vertical integration" the analysis on the diagnostic variables is mapped into the space of the prognostic variables in region described by the diagnostic variables. This does not alter values in the region outside that represented by the diagnostic variables. Both the prognostic background values and the diagnostic analysis values are used to generate a feature preserving (i.e., preserving the features of the original prognostic profile) analysis in the space of the prognostic variables.
6. Treating the prognostic variables that were adjusted during the vertical integration step as hard constraints, an analysis is generated on the balance of the points in the prognostic representation.

A pitfall with this method is that Steps 2 and 5 are reliant on hueristic constructs and are likely to require significant testing and re-work to achieve robust operation.

With all such analysis schemes, determination of background and observation error covariances is a central issue. At the scales we are interested in – up to a few hundred kilometers in range and (generally) lower than 1000 meters, and in the space of modified refractivity in represented in both

Cartesian coordinates and in the diagnostic parameter surfaces, these covariances have not been of interest before. Our approach is to utilize covariances based on parametric equations commonly used in data assimilation and then employ ensemble forecasting and observations to set the parameter values.

WORK COMPLETED

The dual-space objective analysis scheme has been developed in Matlab. At a high level, this includes implementation of diagnostic routines to map COAMPS fields into the space of the diagnostic variables and populating both the prognositc and diagnostic spaces. The framework has been exercised using Exercising framework with simulated refractivity observations as would be provided by refractivity-from-clutter and refractivity-from-radio with background covariance based on *ad hoc* parameter values. An example is shown in Figure 1. A detailed explaination of the figure is as follows:

1. The upper-left plot show refractivity profiles on a 275 km West-to-East cross-section in the southern California basin. The legend in the upper right indicates the definition of symbols used in the plot. The inflection points, minimum M values and so on are used to diagnose the heights of the top and bottom of the trapping layer and subsequently populate the diagnostic variables over the domain.
2. The lower left plot shows the analysis that results from "assimilating" an incresese in the M-excess of 5 M-units at the location of the 5^{th} refractivity profile as a hard constraint. Such a constraint – either hard or soft – would arise from observed signal strengths being higher than that predicted using the NWP background. In the presence of a background error covariance that has non-zero elements for both the top of the trapping layer and the M-excess (both diagnostic variables) and their cross-covariance terms, a change in both parameters can be expected to result from an observed change in the M-excess. In this instance, the incorporation of the constraint increasing the M-excess has resulted in both a lowering and strengthening of the layer, which is an expected behavior.
3. The background covariance determines how the influence of an observation diminish with range. As can be seen in the lower plot, at the far right (Eastern) end of the cross-section, the difference between the background and the analysis is minimal whereas in the region between 0 km and $\sim$ 140 km, the influence is far more substantial. Again, this is the expected behavior.
4. The picture on the lower right shows the location of the path.

We completed a first paper on impementing an objective analysis for two parameters (relative humidity and air-sea-temperature-difference) associated with the atmospheric surface layer [1]. A key result of the work was the indication that radar clutter observations at S-band result in a constraint in the space of those two variables.

Two NWP ensembles in the region of the Hawaiian Islands are used here that are known to have evaporation ducting conditions. The first is a 16-member ensemble on the air-sea boundary layer at 12 am on May 7, 2008, and the second is a 32-member ensemble that correspond to July 26–28, 2008 with 3 hour gaps starting from 12 am UTC. The data that correspond to 12 am UTC May 7, 2008 are shown in Fig 2. Atmospheric parameters shown in that figure are all at 10 m. Sea temperature in general is higher than the air temperature in this dataset. COAMPS outputs at 10 m are used as inputs to NAVSLaM to find the evaporation duct profiles at each location. The average and standard deviation of

duct heights are shown in Fig. 3. Duct height is not very sensitive to ΔT changes where air temperature is less than the sea temperature. The ensemble for July 26–28, 2008 shows similar variations in the standard deviation of atmospheric variables and duct heights, and thus are not shown.

A quadratic metric is defined to measure the fitness of each set of candidate atmospheric variables **m** to predicted values by NWP and inversions of observed clutter power $\mathbf{P}_o$. Here, $\mathbf{m} = [\Delta T, RH]^T$, with atmospheric variables at a height of 10 m . The clutter power fall-off rate does not convey information about the air pressure and absolute value of the wind-speed, and it is a weak function of sea-surface temperature. Hence, these are used directly from NWP.

Analysis of NWP outputs indicates that assuming a range-independent profile for a radius of 20–25 km is reasonable far from the coasts. Simulations in this paper are made by taking the average COAMPS predictions at the location of interest and assuming that the ΔT, humidity and wind profiles are range-independent up to a range of 25 km. The same approach can be extended to range-dependent profile inversions where the state vector will be larger.

The examples in Fig. 4 consider the radar clutter with CNR of 25 dB at the range of 10 km. A 5° azimuthal segment is used for each inversion where synthetic clutter power is generated with independent noises and 1° azimuthal spacing. The logarithmic radar cross section is assumed to have a Gaussian density with zero mean and 3 dB standard deviation. The average of the NWP ensemble is taken as the true state and used to generate 100 clutter power realizations. Synthetic clutter powers in the range of 5–25 km with bins every 1 km are used for RFC-ED inversions and joint NWP, RFC-ED inversions. Two-dimensional and marginal densities of NWP ensemble, RFC-ED inversions and joint inversions are all demonstrated in these plots. Histograms of inverted duct heights obtained from RFC-ED inversions are also plotted.

RESULTS

The key results so far is that we know that we can implement the hybrid analysis at operational scales, on a Windows or Mac laptop and acheive run-times on the order of seconds to a minute or so.

IMPACT/APPLICATIONS

A trend in radar and radio is to enable tapping of device status and data such as as observed power to other devices. For example, clutter power measurements with the SPS-48 E are now provided to down-stream processing to enable display of hazardous weather. RDF in conjunction with inverse methods in EM propagation enables using such data to refine refractivity estimation.

TRANSITIONS

The refractivity data fusion (RDF) has been selected as a Rapid Transition Project under SPAWAR PMW-120 and ONR-322 funding.

REFERENCES

[1] Karimian, A, C Yardim, T Haack, P Gerstoft, WS. Hodgkiss, T Rogers, Towards assimilation of atmospheric surface layer using weather prediction and radar clutter observations, AMS J Applied

Meteorology and Climatology, 2013

[2] Daley, R., Atmospheric Data Analysis, Cambridge University Press, 1991

[3] Kalnay, E., Atmospheric Modeling, Data Assimilation, and Predictability, Cambridge University Press, 341 pp., 2003

PUBLICATIONS

Karimian, A, C Yardim, T Haack, P Gerstoft, WS. Hodgkiss, T Rogers (2013), Towards assimilation of atmospheric surface layer using weather prediction and radar clutter observations, AMS J Applied Meteorology and Climatology, DOI:10.1175/JAMC-D-12-0320.1.

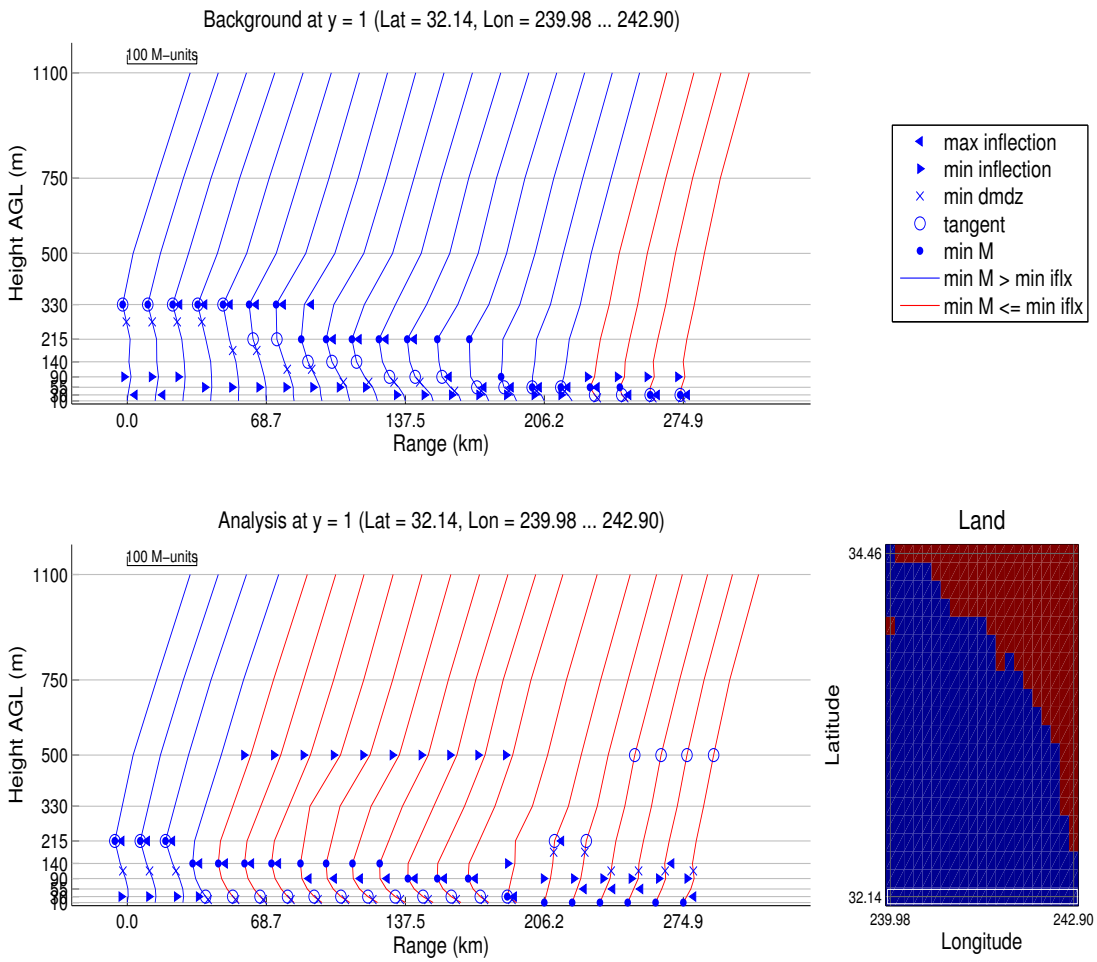

Figure 1: An example of RDF. The top plot shows a range series of refractivity profiles from COAMPS. The bottom plot shows the result of implementing the RDF objective analysis using a constraint that increases the M-excess at the 5th profile from the west (left). A legend is in the upper right indicates the definition of symbols shown in the plot. The values associated with the symbols are used in generating the diagnostic parameters. The picture in the lower right shows the geographic domain with a white line indicating the location of the range series of refractivity profiles. The objective analysis in the space of the diagnostic variables (which includes the M-excess) results in both a lowering of the top of the trapping layer and a more negative average refractivity gradient in the region below the trapping layer. That response is a function of the background covariance and is an expected behavior. Note that the symbol associated with the term "tangent" indicates the point where a line drawn from the value of M at the bottom of the profile becomes tangent with the profile from its left side in the figure.

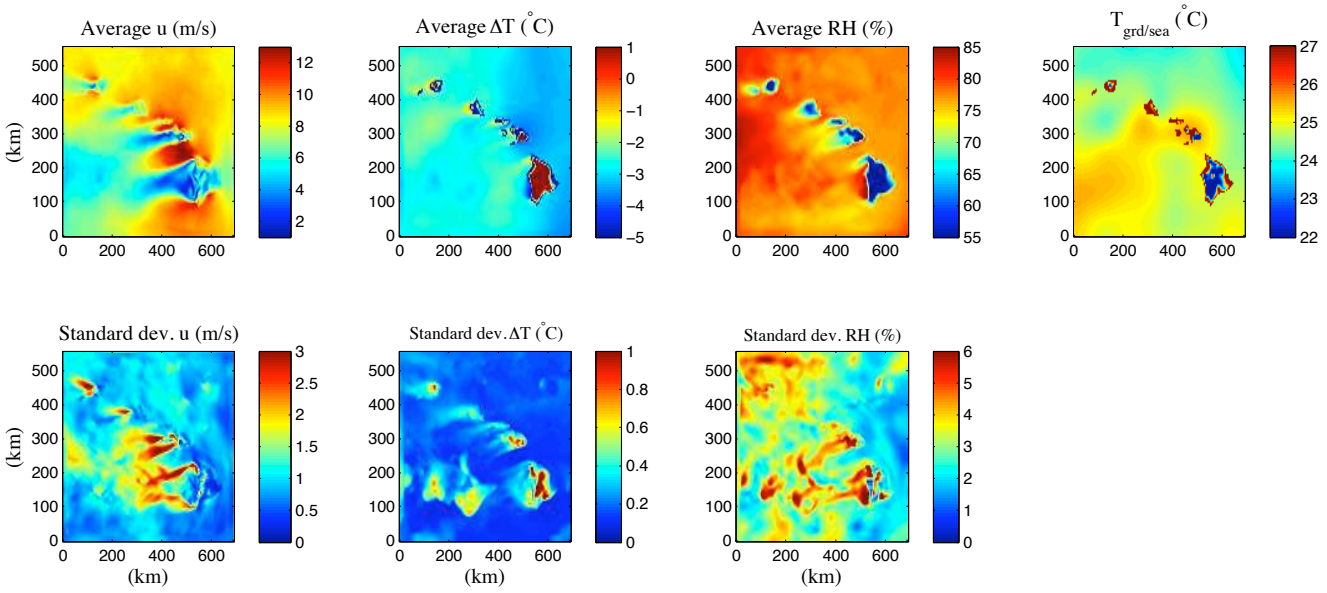

Figure 2: Average values (top row) and standard deviation (bottom row) of COAMPS ensemble of wind-speed, air-sea/ground temperature difference and relative humidity at 10 m around the Hawaii Islands for May 7, 2008 at 12 am UTC using 5 km grid spacings. The last column is the observed surface temperature (sea or ground surface) during the same time using buoy and ship data. For more details see Karimian et al. [2013].

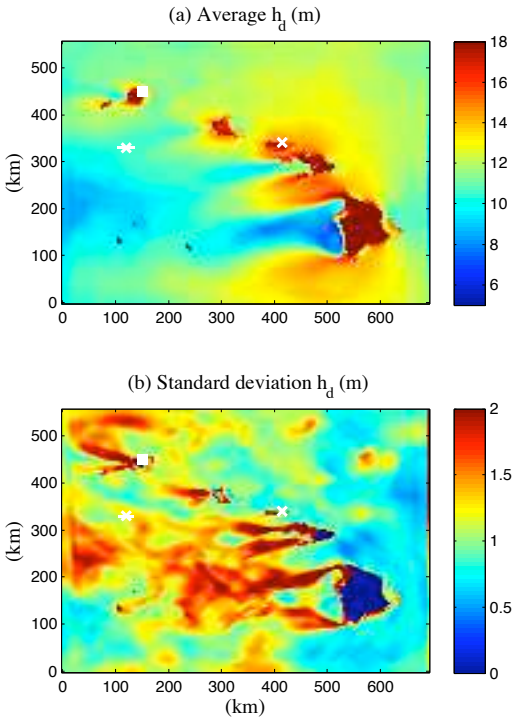

Figure 3: (a) Average and (b) standard deviation of duct heights obtained by running NAVSLaM on the COAMPS ensemble in Fig. 2. The geographic locations of cases analyzed in Figs. 4–?? are marked by white (∗), (×) and (square), respectively. For more details see Karimian et al. [2013].

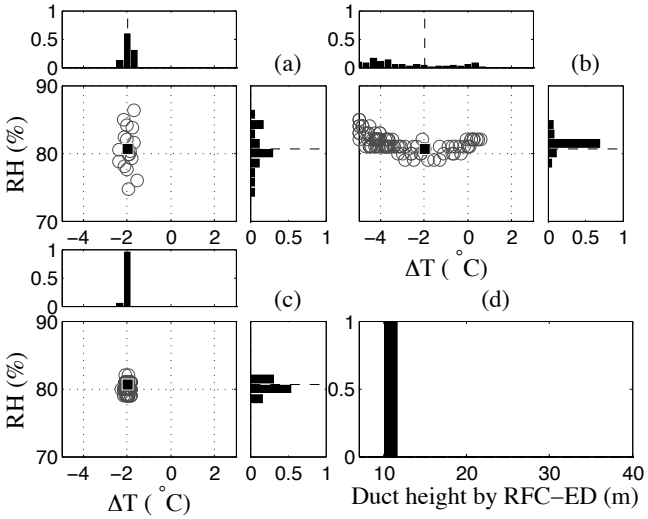

Figure 4: Case 1, $\Delta T < 0$ corresponding to 12 am UTC May 7, 2008 at [120, 330] km in Fig. 2, (a–c): Scatter plots of ΔT and RH, and their marginal densities obtained by (a) COAMPS ensemble, (b) RFC-ED, (c) joint NWP, RFC-ED. The NWP ensemble mean (square) is used for clutter power simulations. (d): Histogram of duct heights obtained by RFC-ED in (b). For more details see Karimian et al. [2013].